

Reaction of hydroquinone with hematite

I. Study of adsorption by electrochemical-scanning tunneling microscopy and X-ray photoelectron spectroscopy

Andrew G. Stack,^{a,*} Carrick M. Eggleston,^a and Mark H. Engelhard^b

^a Department of Geology and Geophysics, University of Wyoming, Laramie, WY 82071-3006, USA

^b William R. Wiley Environmental Molecular Sciences Laboratory, Pacific Northwest National Laboratory, P.O. Box 999, K8-93, Richland, WA 99352, USA

Received 29 August 2003; accepted 12 December 2003

Available online 3 February 2004

Abstract

The reaction of hematite with quinones and the quinone moieties of larger molecules may be an important factor in limiting the rate of reductive dissolution, especially by iron-reducing bacteria. Here, the electrochemical and physical properties of hydroquinone adsorbed on hematite surfaces at pH 2.5–3 were investigated with cyclic voltammetry (CV), electrochemical-scanning tunneling microscopy (EC-STM), and X-ray photoelectron spectroscopy (XPS). An oxidation peak for hydroquinone was observed in the CV experiments, as well as (photo)reduction of iron and decomposition of the solvent. The EC-STM results indicate that hydroquinone sometimes forms an ordered monolayer with ~ 1.1 QH₂/nm², but can be fairly disordered (especially when viewed at larger scales). XPS results indicate that hydroquinone and benzoquinone are retained at the interface in increasing amounts as the reaction proceeds, but reduced iron is not observed. These results suggest that quinones do not adsorb by an inner-sphere complex where adsorbate–surface interactions determine the adsorbate surface structure, but rather in an outer-sphere complex where interactions among the adsorbate molecules dominate.

© 2004 Elsevier Inc. All rights reserved.

Keywords: Hydroquinone; Hematite; α -Fe₂O₃; Reductive dissolution; Biological electron transfer

1. Introduction

Iron is the most common redox-active transition metal in the earth's crust and is involved in a variety of electron-transfer processes, both biological and abiotic. It is potentially the most common terminal electron acceptor used by organisms for respiration after oxygen [1,2] and as such, the sheer quantity of biologically driven iron cycling would make it a subject of substantial environmental interest. Of additional concern is the potential for degradation of environmental contaminants by dissimilatory iron-reducing bacteria (DIRB). Such contaminants include use by DIRB of benzene, toluene, ethylbenzene, and xylene (BTEX) [2–4] compounds as substrates, as well as direct metabolization and/or indirect solubilization of a variety of toxic metals such as technetium(VII) and uranium(VI) [5–8]. It has been

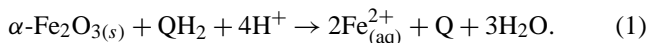
shown that there can be a correlation between bioavailable iron oxides and rates of benzene and toluene degradation by microorganisms [9]. This suggests that one of the controls on the bioavailability of iron oxides and their rate of dissolution may be the interaction of DIRB with an iron oxide surface. Extracellular quinones have been shown to be produced by facultative DIRB to “shuttle” electrons to an iron-oxide surface from the electron-transport chain located in the cell wall [10,11]. While no obligate DIRB have yet been shown to produce extracellular quinones [12], introduced quinones [13] and quinone moieties of humic acids [14] can be used to increase the rate of dissolution of iron oxides.

In this work we report the results of a study of the interaction of hydroquinone (1,4-dihydroxybenzene) with the hematite (α -Fe₂O₃) (0001) surface at pH 2.5–3. This is the first of two companion papers and will focus on the adsorption behavior of hydroquinone; the second will focus on the rate of reduction dissolution of hematite and the calculation of the electron-transfer rate [15]. Hydroquinone itself has not been shown to be utilizable by DIRB [16], but it was chosen

* Corresponding author. Present address: Department of Land, Air and Water Resources, University of California, Davis, CA 95616, USA.
E-mail address: astack@ucdavis.edu (A.G. Stack).

as a study molecule because more is known about its interaction with oxide surfaces and its oxidation steps than for substituted quinones. Hematite was chosen as substrate because it is relatively common in groundwater environments and because it is a semiconductor, which allows us to use a suite of electrochemical techniques not available with other, wide-band-gap iron (hydr)oxides.

The hydroquinone–iron oxide system has been studied previously [17,18] and a general description of the reaction mechanism consists of adsorption of hydroquinone to an iron-surface site, followed by electron transfer (forming a semiquinone radical and a reduced iron), desorption of the semiquinone, and dissolution of the reduced iron. These steps are repeated with the semiquinone radical in place of the hydroquinone and another reduced iron is released with a benzoquinone. The proposed overall reaction stoichiometry is [17,18]



While the exact number of protons involved in the reaction is unknown, it is reasonable to write it as consuming protons at low pH.

At pH 7 it has been shown that hydroquinone adsorbs as an inner-sphere complex via a bridging oxygen [18] (Fig. 1a). For this form of adsorption to occur the hydroquinone must lose a proton prior to adsorbing (in Fig. 1a, a proton is lost from the hydroquinone and a hydroxyl is lost from the surface site). We argue that this process is not

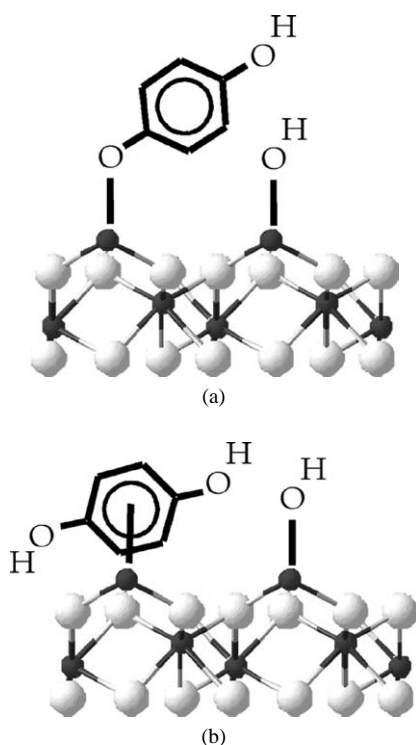


Fig. 1. Illustration of conceivable adsorption behaviors on hematite. Iron atoms are dark gray, oxygen is white, carbon is black, and protons are light gray. (a) Chemisorption via a bridging oxygen [14]. (b) Chemisorption via a π -backbonding complex.

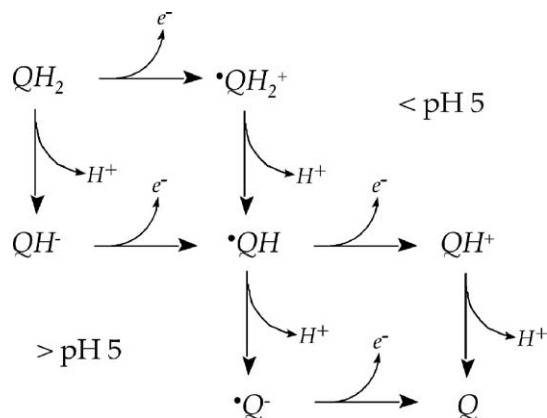


Fig. 2. Pathways for oxidation of hydroquinone (QH_2) through a semiquinone intermediate (QH) to benzoquinone (Q). Oxidation proceeds via the top pathway for pHs < 5 (electron loss followed by proton loss repeated twice, eHeH), and the bottom pathway for pHs > 5 (proton loss followed by electron loss repeated twice, HeHe [15,16]).

likely at low pH due to the pH dependence of the oxidation pathway of hydroquinone, but to demonstrate this some discussion of the oxidation behavior of hydroquinone as a function of pH is needed. Reversible oxidation of hydroquinone involves the loss of two electrons and two protons (Fig. 2), so there are four different likely pathways to the oxidized benzoquinone, depending on what order electron loss and proton loss follow (assuming that the semiquinone radical must be produced, as has been shown at neutral pH [18]). Analysis of anodic current-density–potential curves at varying pHs show that the oxidation of hydroquinone on platinum is first-order with respect to proton concentration at high pH (> 5) and zero order, i.e., independent, at low pH (< 5) [19]. Similar results were found for a dropping mercury electrode, except that the pH of the transition between pathways was somewhat lower ($\sim \text{pH } 4$) [20]. Further evidence for outer-sphere adsorption at low pH comes from Abdul Rahman et al. [21] in the form of energy-dispersive X-ray absorption spectroscopy fine structure; they find that at pH 1.9 no inner-sphere adduct forms as an intermediate between hexaquaairon(III) and hydroquinone in aqueous solution. From these results, we think it likely that the oxidation pathway (Fig. 2) at low pH will be the upper path for both oxidation events, or electron loss followed by proton loss to form semiquinone, and electron loss followed by proton loss again to form benzoquinone (eHeH). At higher pH it will be the lower pathway in both oxidation events: proton loss followed by electron loss, proton loss, electron loss (HeHe). The adsorption behavior of hydroquinone at pH 7 [18] is consistent with the upper oxidation pathway (HeHe) because proton loss occurs prior to electron transfer.

There is one possibility for an inner-sphere type complex after reaction: a π -backbonding complex with an iron(II) (Fig. 1b). Soto et al. [22] have shown that both benzoquinone and hydroquinone form η_4 and η_6 complexes (respectively) on the Pd(111) surface similar to heterogeneous organometallic complexes created with Pt [23], Mn [24],

Ir [25], and Fe(0) [26]. A π -backbonding complex of this type is not likely to form with an iron(III) surface site due to a paucity of electrons: iron(III) does not have enough electron density to contribute much to a π backbond. None of the above-listed heterogeneous species has the d^5 electronic structure of iron(III), but π -backbonding complexes with d^6 metals have been shown to form (specifically Mn(I) [24]). Since iron(II) is d^6 the possibility of a surface π -backbonding iron(II) complex is investigated here.

In this manuscript we test the hypothesis that hydroquinone adsorption onto hematite basal surfaces is observable. We have conducted this study using CV to understand some basic electrochemistry of the system, and we couple this with EC-STM to examine the adsorbate structure. Finally, we use XPS to examine the reaction progress. After the materials and methods are outlined, the results and discussion of each of these experiments is presented.

2. Materials and methods

2.1. Reagents

Reagent-grade hydroquinone (Aldrich) was used without modification. All solutions were prepared and stored in anaerobic environments (<1 ppm O_2 , Forma Scientific Model 1025 Anaerobic System Glove Box; Coy Laboratories Inc. Gas Analyzer). Because hydroquinone can be oxidized by molecular oxygen [5], all DDI water used in this research was purged with nitrogen gas for at least 30 min prior to use and all experiments were performed under nitrogen.

2.2. CV

Cyclic voltammetry was performed on the STM cell prior to imaging (EG&G Princeton Applied Research, Model 263A potentiostat, with EG&G Electrochemistry Suite software). Scan rates and potential ranges were varied to find the best response and limit side reactions. The scan rate for all voltammograms reported here was 25 mV/s. The open-circuit potential was used as the initial and final potential of the sample (versus the reference). Some experiments were illuminated using a 50-W fiber optic lamp (Dolan–Jenner industries).

An oxidized silver wire was used as a quasi-reference electrode, calibrated against a Ag/AgCl (4 M) electrode via a salt bridge of 0.1 M KBrO₃ prior to each STM experiment. A nominal value of the electrode is $\sim +0.3$ V_{NHE} in pH 2.5 acetic acid and 0.01 M NaCl, but measured values had a 0.15-V range. A platinum wire was used as the counter electrode. The working electrodes were constructed by attaching a hematite sample (see [27] for description of the hematite sample) to a roughened metal puck with graphite paint. A contact wire was attached in the same fashion. This assembly was then coated in silicone (Permatex), leaving

only the hematite exposed. The silicone not only isolates the hematite but also creates a hydrophobic surface on which a bead of solution (~ 0.5 ml) is relatively stable. This assembly was used as the fluid cell in all cyclic voltammetry and EC-STM experiments.

2.3. EC-STM

For a brief review of EC-STM and a diagram of the system setup, see Tao [28]. A Molecular Imaging PicoSPM with an A-type scanner (6 μ m) and a Digital Instruments Nanoscope III controller was used. The fluid cell and electrodes used are the same as for the CV; sample potential was controlled with a Molecular Imaging PicoStat. Commercial Apiezon wax-coated Pt:Ir tips were used (Molecular Imaging, Pico, <10 pA leakage current). All experiments with hydroquinone present were performed under nitrogen. Sample potentials were scanned for the most stable imaging conditions, using the cyclic voltammograms as a guide for potentials with small faradaic currents.

EC-cell solution volumes were approximately 0.5 ml. In experiments with hydroquinone present approximately 10–30 μ l of 1 mM hydroquinone solution was added to the fluid cell. After some hours of imaging, evaporation can cause a substantial loss of fluid, so DI H₂O was added periodically to keep the cell volume approximately constant.

2.4. XPS

X-ray photoelectron spectroscopy (XPS) measurements were made at the Wiley Environmental Molecular Sciences Laboratory using a Physical Electronics Quantum 2000 Scanning ESCA Microprobe with focused monochromatic AlK α X-rays (1486.7 eV) as source. The 98-W, 107- μ m-diameter X-rays were rastered over a 1.4 by 0.2 mm rectangle on the sample. Survey scans (not shown) were collected using a pass energy of 117.4 eV. For the Ag3d_{5/2} peak these conditions produce full width at half maximum (FWHM) of better than 1.6 eV. The high-energy-resolution data was collected using a pass energy of 23.5 eV. For the Ag3d_{5/2} these conditions produce a FWHM of better than 0.75 eV. The data were referenced to an energy scale with binding energies for Cu2p_{3/2} at 932.67 ± 0.05 eV and Au4f at 84.0 ± 0.05 eV.

Samples of hematite for the XPS experiments were cleaned using a 10-min sonication in methanol and a 10-min UV exposure ($\lambda = 185$ nm; Jelight Company, Model 342 UVO-Cleaner). After cleaning, samples were placed in a glove bag filled with house nitrogen. Samples were then exposed to hydroquinone (Sigma–Aldrich) by immersion in a 10 mM solution (same composition as the wet-chemical studies) for 15 min, 1 h, and 15 h. After exposure the samples were wicked dry and placed in the sample chamber of the XPS without exposure to the outside atmosphere.

3. Results and discussion

3.1. CV

Cyclic voltammograms for hematite in pH 2.8 acetic acid with 0.01 M NaCl background electrolyte with and without 10^{-3} M hydroquinone are shown in Fig. 3. The primary feature of Fig. 3a is the cathodic current peak at ~ -0.1 to -0.2 V, the area of which is increased when the sample is illuminated (labeled 1). Upon illumination, photons with energy greater than the band gap (2.2 eV for hematite, see, e.g., [29]; therefore wavelength ≤ 540 nm) will excite electrons from the valence band into the conduction band. An estimate of the flat-band potential of single-crystal hematite at pH 2.8 is $+0.1$ V_{Ag wire} ([31]; corrected for pH). While flat-band potential measurements can vary substantially between experiments [30], this value is consistent with our result. Given the donor density of the hematite used in this study ($\sim 5.5 \times 10^{16}$ cm⁻³; see [27]), the conduction

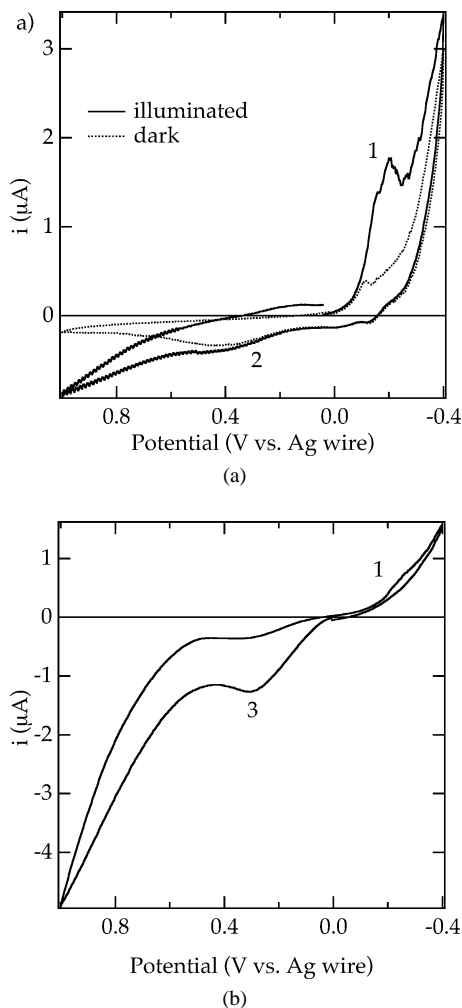


Fig. 3. Cyclic voltammetry data, current versus potential of the quasi-reference electrode. Scan rate is 25 mV/s, pH 2.8 acetic acid, 0.01 M NaCl. (a) Hematite in the dark and illuminated. Peak 1 is reduction of iron; peak 3 is an anomaly. (b) Hematite with 0.001 M hydroquinone (after 15 min). Peak 3 is hydroquinone oxidation.

band should be 100–200 mV negative of the flat-band potential [32]. This translates to a conduction band edge located at approximately -0.1 to -0.2 V_{Ag wire}, where peak 1 is located. Photoemission studies have found that the hematite conduction band is mostly Fe3d in character [33]; therefore, peak 1 is likely indicating reduction of iron(III) at the bottom of the conduction band or surface states that reside in the band gap near the conduction band. This interpretation is consistent with ultraviolet photoelectron spectroscopy measurements of photoexcited hematite [34].

The anodic peak labeled 2 in Fig. 3a is probably an artifact. The hematite sample and electrodes had been exposed to hydroquinone prior to this experiment and there may have been some residual hydroquinone present that was not removed during the cleaning process. An alternate explanation is perhaps that the peak represents the decomposition of the acetate buffer or some reaction with the silicone in the EC cell.

The cathodic and anodic peaks at the extreme potentials represent decomposition of the solvent (e.g., reduction and oxidation of water species, resp.). An increased oxidative current is observed when the hematite is illuminated (anodic current at oxidizing potentials near $+1$ V_{Ag wire}). This photolysis of the solvent has been observed previously on hematite [35].

When hydroquinone is introduced to the cell (Fig. 3b), peak 3 appears. This peak is thought to represent oxidation of hydroquinone to benzoquinone (the semiquinone intermediates are not very stable at this pH [36]). The reduction potential of hydroquinone under these conditions should be approximately $+0.2$ V_{Ag wire}, which is consistent with what is observed. Unfortunately, due to double-layer charging effects and solvent decomposition, it is impractical to integrate the peak area to determine surface layer coverage.

The presence of the oxidation peak with the concomitant lack of the reduction peak is not easily explainable. An *n*-type semiconductor such as this hematite sample should be rectifying and only reduce adsorbates because the formation of a near-surface depletion layer forbids oxidation, except at very positive substrate potentials (see, e.g., [37]). Here, the opposite from what is expected is observed: an oxidation peak with no corresponding reduction. However, if the reduction potential of a redox molecule is near the conduction band edge both oxidations and reductions would be expected to be observed, due to overlap of the redox density of states with the semiconductor's conduction band edge [29]. This is the case here; the reduction potential of hydroquinone ($\sim +0.2$ V_{Ag wire}) is close to the conduction band edge of the hematite, estimated above at -0.1 to -0.2 V_{Ag wire}. Furthermore, when the reduction potential of the redox molecule is similar to the electrode, the peak splitting can sometimes be quite large. Kohl and Bard observed a separation of oxidation and reduction peaks (ΔE_p) of 3.7 V (!) for hydroquinone on *n*-GaP [38]. In this case the oxidation reaction peak center was at a potential close to the conduction band edge and the reduction peak center

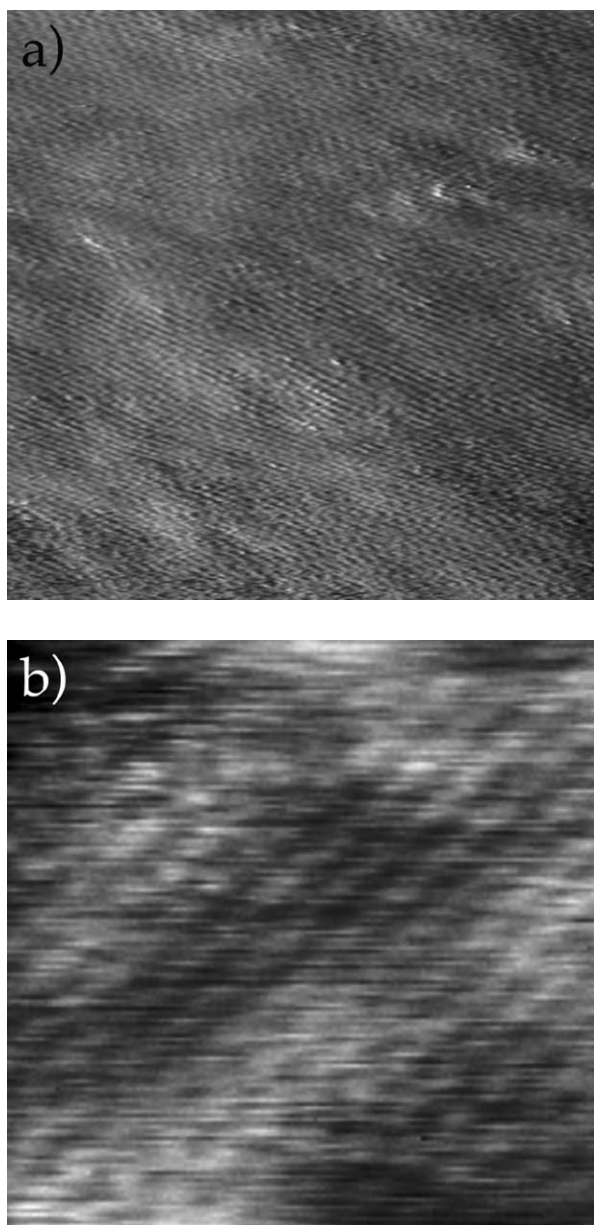


Fig. 4. EC-STM images, pH 2.8 acetic acid, 0.01 M NaCl. (a) A 15-nm scan of hematite in aqueous solution; sample bias is -250 mV, setpoint is 250 pA, z -scale is 0.5 nm, and the sample potential is -0.02 V_{Ag wire}. The characteristic 5-Å periodicity of the hematite unit cell is shown. (b) A 15-nm scan showing the surface after introduction of hydroquinone; the 5-Å periodicity has been replaced by a 1.1-nm periodicity. Sample bias is -100 mV, setpoint is 100 pA, z -scale is 0.2 nm, and sample potential is $+0.18$ V_{Ag wire}.

at a much more negative potential. If such were the case for hematite we would not expect to see the reduction peak due to decomposition of the solvent (Kohl and Bard [38] worked in acetonitrile to avoid this problem).

3.2. EC-STM

Fig. 4a is an image of hematite showing a characteristic 5-Å periodicity (in pH 2.8 acetic acid in 0.01 M NaCl elec-

trolyte, with a sample potential of -0.02 V_{Ag wire} (see, e.g., [27,39,40]). Fig. 4b shows a surface after the introduction of hydroquinone into the STM fluid cell. The 5-Å periodicity has been replaced by a well-ordered hexagonal closest packed 1.1 nm periodicity, similar to hydroquinone monolayers on Pd(111) [41,42]. This is approximately twice the periodicity of iron atoms on the hematite $\langle 001 \rangle$. The error in distance measurements with STM data can be substantial due to drift and scanner creep, so the periodicity of the hydroquinone-covered surface can be considered commensurate with the hematite unit cell. This interpretation leaves open the possibility that there is a strong, specific interaction between quinones and iron surface sites. However, since a closest packed monolayer is observed, it implies either that interadsorbate interactions dominate the adsorbate structure or that hydroquinone adsorbs onto essentially every possible hematite surface site.

If there is not a strong interaction between the adsorbate and the surface (i.e., the hydroquinone forms an outer-sphere complex), the dominant interactions would be hydrogen bonds between quinone molecules and dispersion forces. In crystalline hydroquinone, the interaction energy is determined by a combination of the two [43]. Within the plane of the carbon ring, the intermolecular distances in α -hydroquinone [44] and quinhydrone [45] are approximately 7.2 Å, which is shorter than the 1.1-nm periodicity that is measured in the STM experiments. However, three-dimensional crystal data may not be indicative of two-dimensional structure on a surface. It is also possible that the intermolecular interaction of a monolayer on an oxide surface may consist of some hydrogen bonding among quinones and some hydrogen bonding between quinone molecules and the oxide surface, which will affect a monolayer structure.

Fig. 5 shows images in which a quinone monolayer has a domain of differing structure within the image, rotated $\sim 60^\circ$. Observation of a domain with different structure within a single image is important when STM data are considered because it indicates that the apparent monolayer is probably real and not an artifact produced by the tip. If the apparent monolayer were in fact the result of a multiple tip or a blunt tip, the same feature would reproduce over an entire image.

The well-ordered monolayer shown in Figs. 4 and 5 is not observed with high frequency. A more common result is shown in Fig. 6, where there exists no long-range ordering on the surface. There are some areas on the terraces where something similar to a 1.1-nm periodicity can be seen, but other places where there is no visible ordering. Fig. 6b shows no visible ordering whatsoever. A lack of ordering in some cases and not in others is not unexpected; when the interaction between the surface and the adsorbate or between adsorbate molecules is weak it can be quite difficult to determine what factors or conditions are most influential for forming an ordered monolayer. For example, He et al. [46] found that ordered monolayers of porphyrin on gold only form at certain potentials; otherwise disordered monolayers

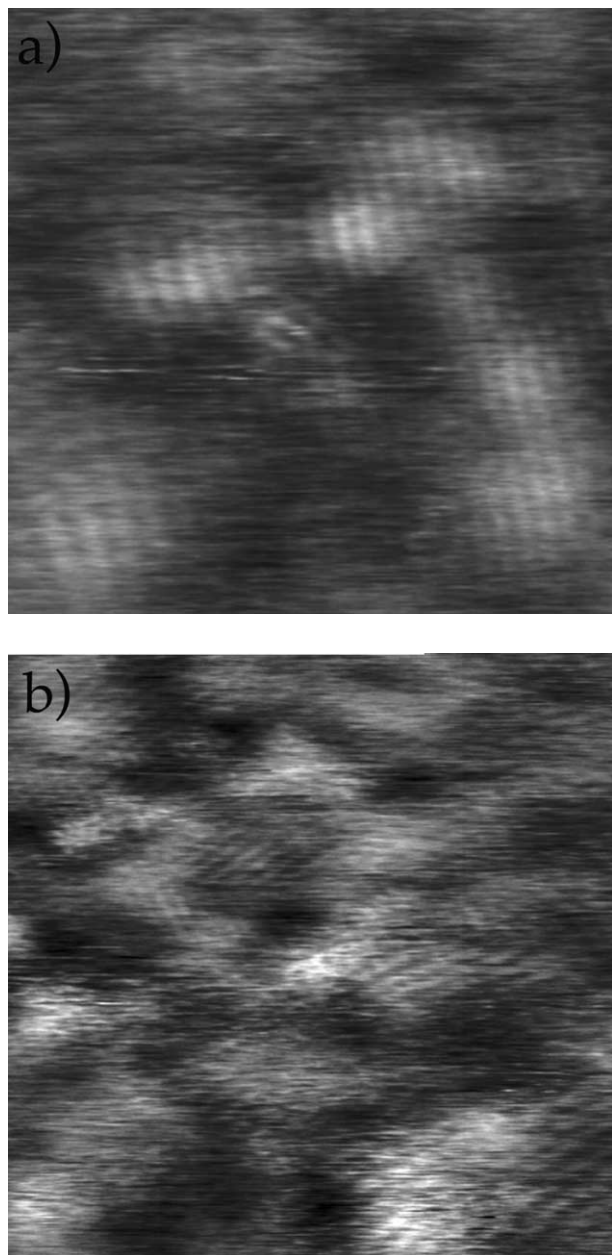


Fig. 5. EC-STM images, pH 2.8 acetic acid, 0.01 M NaCl; sample biases are -100 mV, setpoints are 100 pA, and z -scales are 0.3 nm. (a) A 30 -nm scan; sample potential is -0.02 V_{Ag wire}. Slightly upward, and to the left of the center is an area with structure rotated 60° with respect to the rest of the image. (b) A 40 -nm scan; sample potential is -0.22 V_{Ag wire}. Slightly upward and to the left of center is an area of rotated structure.

form, or no adsorption at all occurs. It is possible that a similar phenomenon is occurring here since varying potentials during deposition were not thoroughly investigated (imaging became quite unstable at any sample potential near where large faradaic currents occur in Fig. 3).

Fig. 7 shows hematite after it has been reacted with hydroquinone over several imaging sessions (10 – 15 h exposure, with varying sample potentials). The surface of the hematite is pitted. The measured depth of the pits is only 0.3 Å, indicating that dissolution has probably resulted

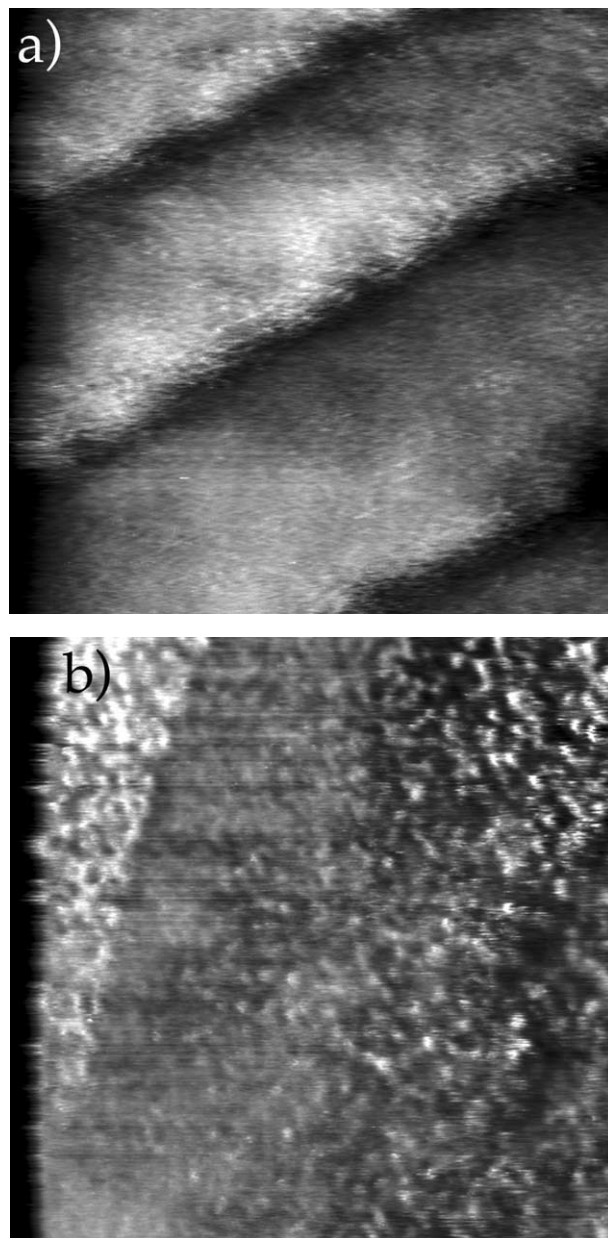


Fig. 6. EC-STM images, pH 2.8 acetic acid, 0.01 M NaCl. (a) Hydroquinone on hematite, 50 -nm scan: sample bias is -250 mV, setpoint is 250 pA, z -scale is 0.5 nm, and sample potential is -0.02 V_{Ag wire}. The steps are monolayer height on hematite (2.3 Å). On the terraces, some areas are ordered (1.1 -nm periodicity), whereas others have no discernable ordering. (b) Hydroquinone on hematite, 100 -nm scan: sample bias is -500 mV, setpoint is 500 pA, z -scale is 0.5 nm and sample potential is -0.20 V_{Ag wire}. No ordering is discernable. The bright feature is a monolayer step of the hematite.

in a difference in terminations of the hematite (i.e., Fe- vs O-termination). Using a resonant tunneling model, Eggleston et al. [27] suggest that in this case the higher terraces are composed of an Fe-termination and the pits are O-terminated. This sample had been exposed to sample potentials where reduction of the surface could occur (see Fig. 3a), so some or all of the dissolution may be attributable to this.

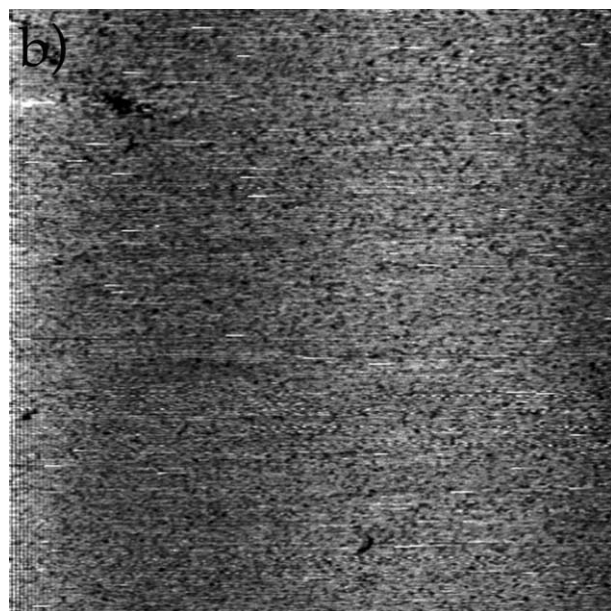
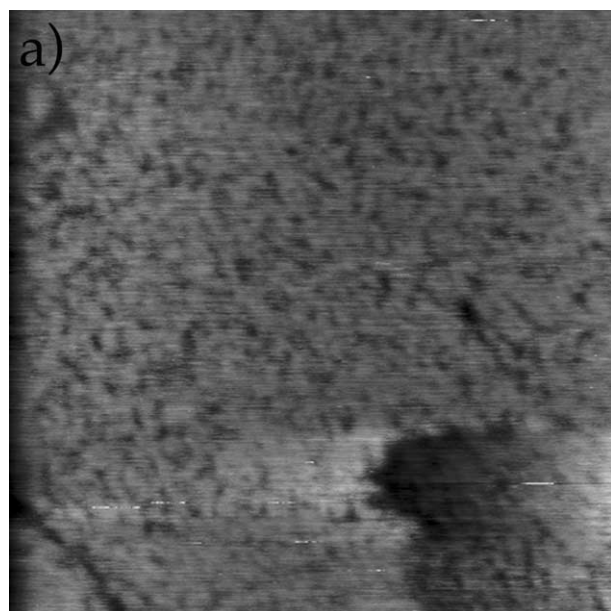


Fig. 7. EC-STM images of hematite after several imaging sessions: pH 2.8 acetic acid, 0.01 M NaCl. Pit depth is 0.3 Å. It is probable that the topmost layer of iron has been stripped away, leaving an oxygen-terminated surface [27]. (a) A 100-nm scan: sample bias is +250 mV, setpoint is 250 pA, z-scale is 0.2 nm, sample potential is 0.03 V_{Ag wire}. (b) Same conditions as in (a), but 250-nm scan size.

3.3. XPS

Fig. 8a shows the carbon 1s spectra as a function of exposure time. With increasing exposure time there is an appearance and (relative) growth of a carbon double-bond oxygen (C=O) peak and a carbon single-bond oxygen (C–O) peak (the C–C, C–H peaks show no trend). The appearance and growth of the C–O peak suggests that hydroquinone has adsorbed onto the hematite surface. While it is somewhat surprising that there is an apparent increase in the surface C–O

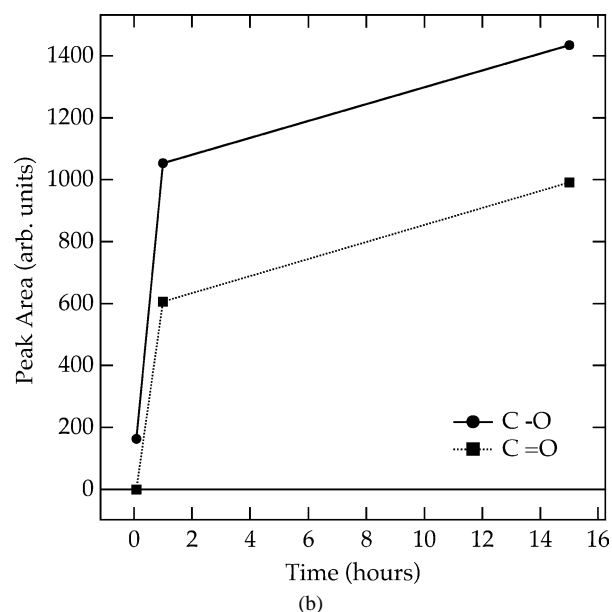
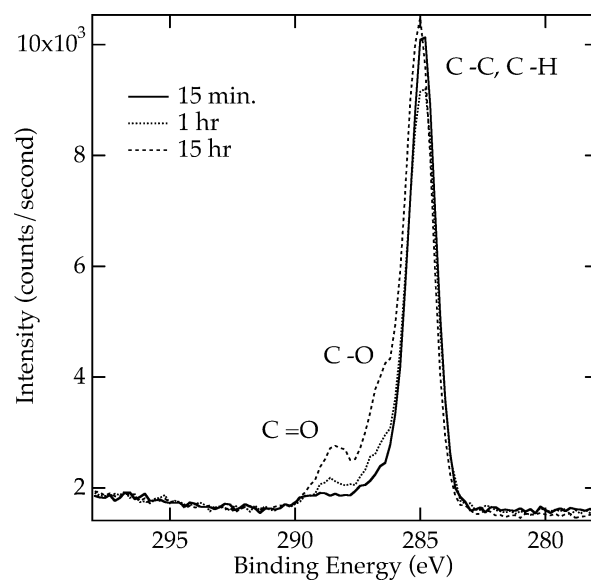


Fig. 8. XPS data of hematite samples. (a) Carbon 1s spectra after exposure to varying amounts of pH 2.5 acetic acid, 0.01 M NaCl, 1 mM hydroquinone. With increased exposure a C–O and C=O peak appear and grow. (b) Peak areas as a function of time using a Lorentzian peak deconvolution (not shown) from the C–O and C=O peaks in (a) after being normalized to the C–C, C–H peak. The C–C and C–H peaks show no trend. Lines are intended as a guide for the eye.

concentration between 1 and 15 h reaction time, it is within expectation: previous workers used a 6-h equilibration time to allow complete adsorption of hydroquinone and catechol on alumina [47]. It is conceivable that hydroquinone is precipitating, but since the solubility is 0.645 M [48] and the concentration of hydroquinone is 10^{-3} M, this is unlikely.

The C=O peak most likely indicates the appearance of benzoquinone on the surface as the reaction progresses. In the absence of significant amounts of oxygen, it is likely that the benzoquinone has been formed by reaction of hy-

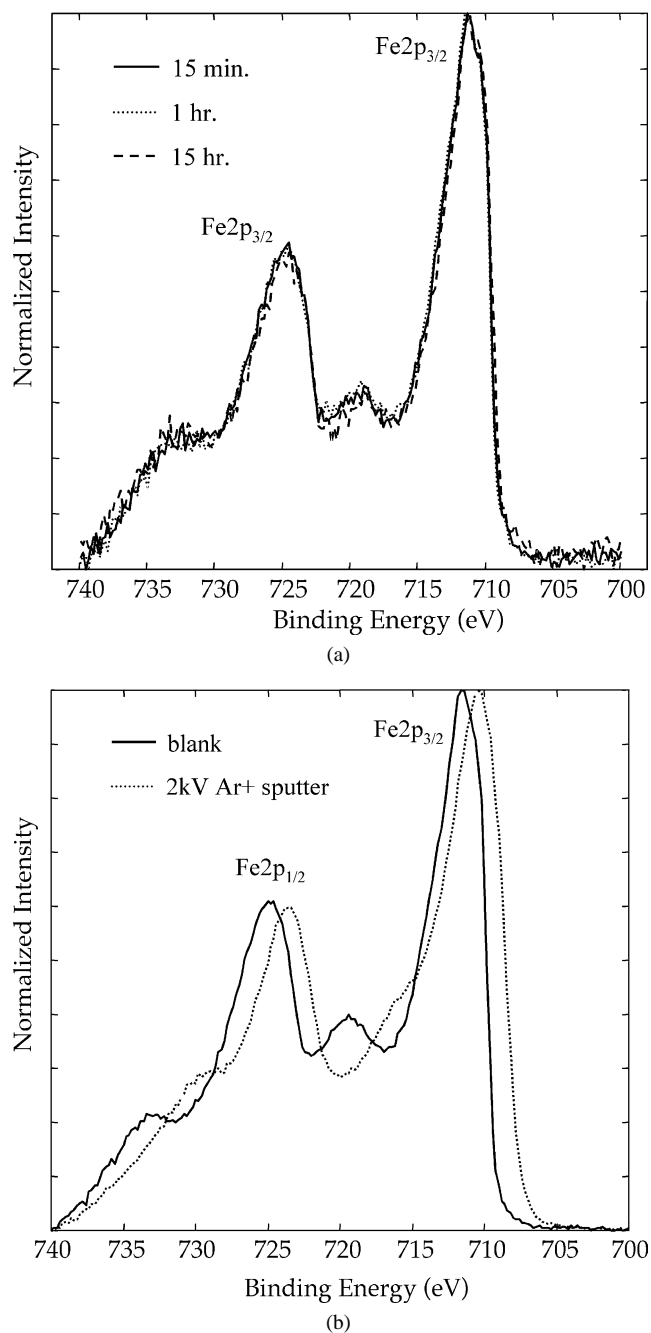


Fig. 9. XPS data of the same samples as in Fig. 8. (a) $Fe2p$ spectra. No detectable $Fe(II)$, which would appear as a peak or shoulder on the lower binding energy side of the $Fe2p$ peaks and a shift in the position of the satellites [49]. (b) Separate samples before and after sputtering with argon at 2 kV at 2 nm/min for 2 min. Reduced iron is observed [49].

droquinone with the iron oxide sample. It is unlikely that any precipitate containing benzoquinone is forming; the K_{sp} of quinhydrone (a 1:1 mixture of hydroquinone and benzoquinone) is 0.289 M [48], and the K_{sp} of benzoquinone is 0.127 M [48] (see [15] for example concentrations of benzoquinone species during reaction with a hematite powder).

Fig. 9a shows the $Fe2p$ spectra for the same samples. There is no indication of $Fe(II)$ on the surface. Reduced iron would appear as a shoulder on the low-binding-energy

side of the $Fe2p_{3/2}$ peak and the positions of the satellites would shift [49]. To verify that $Fe(II)$ could be detected by XPS, a separate sample was sputtered with argon. Bombardment of $\alpha-Fe_2O_3$ surfaces with Ar^+ ions has been shown to preferentially remove oxygen atoms and concomitantly reduce ferric iron, creating FeO [49]. In our case, sputtering clearly shows the features of $Fe(II)$ on the surface (Fig. 9b). Thus, if $Fe(II)$ were accumulating on the surface (approximately >5 atom %), it would probably have been detected. The lack of observation of any $Fe(II)$ on the surface, while benzoquinone was detected, indicates that a π -backbonding complex between $Fe(II)$ and benzoquinone is probably not forming (Fig. 1b). This complex may form in solution or may exist only briefly on the surface, but it is not likely that this complex represents the dominant interaction between benzoquinone and iron surface sites.

It is conceivable that electrons donated to hematite (by hydroquinone) are delocalized (i.e., injected into the conduction band rather than onto a particular site). In this case, only high-energy sites would dissolve, not necessarily the sites that the electron has been transferred to. Thus, there would not necessarily be any $Fe(II)$ observed on the (basal) surface studied in this experiment. However, based on charge-carrier mobility measurements and the energy of activation for electron transfer, the conductivity behavior of hematite is better described by a localized electron model (i.e., a small polaron), not a delocalized band model (see, e.g., [50,51]). A more likely explanation of the results in Fig. 9 is that $Fe(II)$ is not retained substantially on the surface during reductive dissolution; it has been shown that $Fe(II)$ does not adsorb well onto goethite at low pHs [52] and hematite is expected to behave in a similar fashion. The presence of the benzoquinone on the surface and the lack of $Fe(II)$ indicate that $Fe(II)$ removal from the surface is probably not rate limiting. If it were, then there would be twice as much $Fe(II)$ on the surface as benzoquinone. By the same argument, the presence of benzoquinone on the surface indicates that its removal from the surface is relatively slow and that adsorption of hydroquinone/desorption of benzoquinone should not be ruled out immediately as a candidate for the rate-limiting step.

4. Summary

Adsorption of hydroquinone onto hematite basal surfaces has been studied using CV, EC-STM, and XPS. The CV showed irreversible oxidation of hydroquinone to benzoquinone as well as reduction of iron. EC-STM experiments showed that a monolayer of hydroquinone sometimes forms with an apparent packing density of ~ 1.1 QH_2/nm^2 , similar to hydroquinone monolayers on platinum and palladium. At larger scales, the monolayer appears to be much more disordered. The results of the XPS experiments show that, while hydroquinone and benzoquinone are retained on the surface, ferrous iron is not, implying that metal detachment

is not rate-limiting. These results suggest that interadsorbate interactions dominate the monolayer structure, as opposed to adsorbate–surface interactions.

Acknowledgments

This research was supported by NSF Career Grant EAR-9875830 to CME and DOE-PNNL EMSL User Grant 2554. A portion of this research was performed at the W.R. Wiley Environmental Molecular Sciences Laboratory, a national scientific user facility sponsored by the U.S. Department of Energy's Office of Biological and Environmental Research and located at Pacific Northwest National Laboratory. Pacific Northwest National Laboratory is operated for the DOE by Battelle Memorial Institute under Contract DE-AC06-76RLO 1830.

References

- [1] D.R. Lovley, E.F. Phillips, D.J. Lonergan, *Environ. Sci. Technol.* 25 (1991) 1062.
- [2] D.R. Lovley, *Microbiol. Rev.* 55 (1991) 259.
- [3] I.M. Cozzarelli, B.A. Bekins, M.J. Baedecker, G.R. Aiken, R.P. Eganhouse, M.E. Tuccillo, J. Contam. Hydrogeol. 53 (2001) 369.
- [4] B.A. Bekins, I.M. Cozzarelli, E.M. Godsy, E. Warren, H.I. Essaid, M.E. Tuccillo, J. Contam. Hydrogeol. 53 (2001) 387.
- [5] J.K. Frederickson, J.M. Zachara, D.W. Kennedy, M.C. Duff, Y.A. Gorby, S.-M.W. Li, K.M. Krupka, *Geochim. Cosmochim. Acta* 64 (2001) 3085.
- [6] J.R. Lloyd, F.R. Livens, D.R. Lovley, J. Chesnes, S. Glasauer, D.J. Bunker, *Geomicrobiol. J.* 19 (2001) 103.
- [7] J.R. Lloyd, V.A. Sole, C.V. Van Praagh, D.R. Lovley, *Appl. Environ. Microbiol.* 66 (2000) 3743.
- [8] D.R. Lovley, E.J.P. Phillips, Y.A. Gorby, E. Landa, *Nature* 350 (2001) 413.
- [9] J.R. Rogers, P.C. Bennett, W.J. Choi, in: *Proceedings of the Tenth International Symposium on Water–Rock Interaction WRI-10, Vil-lasimus, Italy, 10–15 July, 2001*.
- [10] D.K. Newman, R. Colter, *Nature* 405 (2000) 94.
- [11] M.E. Hernandez, D.K. Newman, *Cell Mol. Life Sci.* 58 (2001) 1562.
- [12] K.P. Nevin, D.R. Lovley, *J. Bacteriol.* 181 (2000) 7647.
- [13] J.M. Zachara, J.K. Fredrickson, S.-M. Li, D.W. Kennedy, S.C. Smith, P.L. Gassman, *Am. Mineral.* 83 (1998) 1426.
- [14] D.T. Scott, D.M. McKnight, E.L. Blunt-Harris, S.E. Kolesar, D.R. Lovley, *Environ. Sci. Technol.* 32 (1998) 2984.
- [15] A.G. Stack, K.M. Rosso, C.M. Eggleston, *J. Colloid Interface Sci.*, in press.
- [16] R.A. Royer, W.D. Burgos, A.S. Fisher, R.F. Unz, B.A. Dempsey, *Environ. Sci. Technol.* 36 (2002) 1930.
- [17] J.S. LaKind, A.T. Stone, *Geochim. Cosmochim. Acta* 53 (1989) 961.
- [18] K.-H. Kung, M.B. McBride, *Clays Clay Miner.* 36 (1988) 303.
- [19] K.J. Vetter, *Electrochemical Kinetics, Theoretical and Experimental Aspects*, Academic Press, New York, 1967.
- [20] J.M. Hale, R. Parsons, *Trans. Faraday Soc.* 59 (1962) 1429.
- [21] M.B.B. Abdul Rahman, P.R. Bolton, J. Evans, A.J. Dent, I. Harvey, S. Diaz-Moreno, *Faraday Discuss.* 122 (2002) 211.
- [22] J.E. Soto, Y.-G. Kim, M.P. Soriaga, *Electrochem. Commun.* 1 (1999) 135.
- [23] U. Belluco, *Organometallic and Coordination Chemistry of Platinum*, Academic Press, London, 1974.
- [24] S. Sun, G.B. Carpenter, D.A. Sweigart, *J. Organomet. Chem.* 512 (1996) 257.
- [25] J. Le Bras, H. Amouri, J. Vaisserman, *Organometallics* 17 (1998) 1116.
- [26] H.W. Sternberg, R. Markby, I. Wender, *J. Am. Chem. Soc.* 80 (1958) 1009.
- [27] C.M. Eggleston, A.G. Stack, K.M. Rosso, S.R. Higgins, A.M. Bice, S.W. Boese, R.D. Pribyl, J.J. Nichols, *Geochim. Cosmochim. Acta* 67 (2003) 985.
- [28] N.J. Tao, *Phys. Rev. Lett.* 76 (1996) 4066.
- [29] A.J. Nozik, *Annu. Rev. Phys. Chem.* 29 (1978) 189.
- [30] D. Wei, K. Osseo-Asare, *J. Electrochem. Soc.* 143 (1996) 3192.
- [31] R.K. Quinn, R.D. Nasby, R.J. Baughman, *Mater. Res. Bull.* 11 (1976) 1011.
- [32] S.N. Frank, A.J. Bard, *J. Am. Chem. Soc.* 97 (1975) 7427.
- [33] R.J. Lad, V.E. Henrich, *Phys. Rev. B* 39 (1989) 13478.
- [34] D.S. Toledano, E.R. Dufresne, V.E. Henrich, *J. Vac. Sci. Technol. A* 16 (1998) 1050.
- [35] K.L. Hardee, A.J. Bard, *J. Electrochem. Soc.* 123 (1976) 1024.
- [36] C.A. Bishop, L.K.J. Tong, *J. Am. Chem. Soc.* 87 (3) (1965) 501.
- [37] S.R. Morrison, *Electrochemistry at Semiconductor and Oxidized Metal Electrodes*, Plenum, New York, 1990.
- [38] P.A. Kohl, A.J. Bard, *J. Am. Chem. Soc.* 99 (23) (1977) 7531.
- [39] C.M. Eggleston, *Am. Mineral.* 84 (1999) 1061.
- [40] U. Becker, M.F.J. Hochella, E. Aprà, *Am. Mineral.* 81 (1996) 1301.
- [41] Y.-G. Kim, M.P. Soriaga, *J. Colloid Interface Sci.* 236 (2001) 197.
- [42] J.E. Soto, Y.-G. Kim, M.P. Soriaga, *Electrochem. Commun.* 1 (1999) 135.
- [43] K. Suzuki, S. Seki, *Bull. Chem. Soc. Jpn.* 26 (1953) 372.
- [44] S.C. Wallwork, H.M. Powell, *J. Chem. Soc. Perkin II* 4 (1980) 641.
- [45] H. Matsuda, K. Osaki, I. Nitta, *Bull. Chem. Soc. Jpn.* 31 (1958) 611.
- [46] Y. He, Y. Tao, E. Bourget, *J. Am. Chem. Soc.* 124 (2002) 11964.
- [47] M.B. McBride, L.G. Wesselink, *Environ. Sci. Technol.* 22 (1987) 703.
- [48] F.S. Granger, J.M. Nelson, *J. Am. Chem. Soc.* 43 (1921) 1407.
- [49] N.S. McIntyre, D.G. Zetaruk, *Anal. Chem.* 49 (1977) 1521.
- [50] K.M. Rosso, D.A.M. Smith, M. Dupuis, *J. Chem. Phys.* 118 (2003) 6455.
- [51] J.B. Goodenough, *Prog. Sol. Sci. Chem.* 5 (1972) 145.
- [52] C.G. Allen, C. Kirby, M. Sellers, *J. Chem. Soc. Faraday Trans.* 84 (1988) 355.